



UvA-DARE (Digital Academic Repository)

Modeling pulsed dye laser treatment of psoriatic plaques by combining numerical methods and image-derived lesion morphologies

Wilk, L.S.; Doppegieter, M.; van der Beek, N.; van Leeuwen, T.G.; Aalders, M.C.G.

DOI

[10.1002/lsm.23781](https://doi.org/10.1002/lsm.23781)

Publication date

2024

Document Version

Final published version

Published in

Lasers in Surgery and Medicine

License

CC BY-NC-ND

[Link to publication](#)

Citation for published version (APA):

Wilk, L. S., Doppegieter, M., van der Beek, N., van Leeuwen, T. G., & Aalders, M. C. G. (2024). Modeling pulsed dye laser treatment of psoriatic plaques by combining numerical methods and image-derived lesion morphologies. *Lasers in Surgery and Medicine*, 56(5), 508-522. <https://doi.org/10.1002/lsm.23781>

General rights

It is not permitted to download or to forward/distribute the text or part of it without the consent of the author(s) and/or copyright holder(s), other than for strictly personal, individual use, unless the work is under an open content license (like Creative Commons).



Disclaimer/Complaints regulations

If you believe that digital publication of certain material infringes any of your rights or (privacy) interests, please let the Library know, stating your reasons. In case of a legitimate complaint, the Library will make the material inaccessible and/or remove it from the website. Please Ask the Library: <https://uba.uva.nl/en/contact>, or a letter to: Library of the University of Amsterdam, Secretariat, P.O. Box 19185, 1000 GD Amsterdam, The Netherlands. You will be contacted as soon as possible.

UvA-DARE is a service provided by the library of the University of Amsterdam (<https://dare.uva.nl>)

BASIC SCIENCE ARTICLE

Modeling pulsed dye laser treatment of psoriatic plaques by combining numerical methods and image-derived lesion morphologies

Leah S. Wilk PhD^{1,2,3}  | Meagan Doppegieter MSc^{1,4}  | Nick van der Beek MSc⁵ |
Ton G. van Leeuwen PhD^{1,6,7} | Maurice C. G. Aalders PhD^{1,2,3}

¹Amsterdam UMC, location University of Amsterdam, Biomedical Engineering and Physics, Amsterdam, The Netherlands

²Co van Ledden Hulsebosch Center, University of Amsterdam, Amsterdam, The Netherlands

³Amsterdam Public Health, Methodology, Amsterdam, The Netherlands

⁴Amsterdam Cardiovascular Sciences, Microcirculation, Amsterdam, The Netherlands

⁵ZBC MultiCare, Independent Treatment Center for Dermatology, Hilversum, The Netherlands

⁶Amsterdam Cardiovascular Sciences, Heart Failure and Arrhythmias, Amsterdam, The Netherlands

⁷Cancer Center Amsterdam, Imaging and Biomarkers, Amsterdam, The Netherlands

Correspondence

Maurice C. G. Aalders, PhD, Amsterdam UMC, location University of Amsterdam, Biomedical Engineering and Physics, Meibergdreef 9, 1105AZ Amsterdam, The Netherlands.

Email: m.c.aalders@amsterdamumc.nl

Abstract

Objectives: Knowledge of the physical effects of pulsed dye laser (PDL) treatment of psoriatic lesions is essential in unraveling the remedial mechanisms of this treatment and hence also in maximizing in its disease-modifying potential. Therefore, the main objective of this study was to provide estimates of these physical effects (for laser wavelengths of 585 and 595 nm), with the aim of identifying pathogenic processes that may be affected by these conditions.

Methods: We modeled the laser light propagation and subsequent photothermal heating by numerically solving the transient diffusion and heat equations simultaneously. To this end, we used the finite element method in conjunction with an image-derived psoriatic lesion morphology (which was defined by segmenting blood vessels from a confocal microscopy image of a fluorescently labeled section of a 3 mm punch biopsy of a psoriatic lesion). The resulting predictions of the generated temperature field within the lesion were then used to assess the possibility of stalling or arresting some suspected pathogenic processes.

Results: According to our results, it is conceivable that perivascular nerves are thermally denatured, as almost all locations that reach 60°C were found to be within 18 μm (at 585 nm) and 11 μm (at 595 nm) of a blood vessel wall. Furthermore, activation of TRPV1 and TRPV2 channels in perivascular neuronal and immune cells is highly likely, since a critical temperature of 43°C is generated at locations within up to 350 μm of a vessel wall (at both wavelengths) and sustained for up to 700 ms (at 585 nm) and 40 ms (at 595 nm), while a critical temperature of 52°C is reached by locations within 80 μm (at 585 nm) and 30 μm (at 595 nm) of a vessel wall and sustained for up to 100 ms (at 585 nm) and 30 ms (at 595 nm). Finally, we found that the blood vessel coagulation-inducing temperature of 70°C is sustained in the vascular epithelium for up to 19 and 5 ms at 585 and 595 nm, respectively, rendering partial or total loss of vascular functionality a distinct possibility.

Conclusions: The presented approach constitutes a useful tool to provide realistic estimates of the photothermal effects of PDL treatment of psoriatic plaques (as well as other selective photothermolysis-based treatments), yielding information that is essential in guiding future experimental studies toward unraveling the remedial mechanisms of these treatments.

KEYWORDS

finite element method, heat transport, laser treatment, light transport, psoriasis

This is an open access article under the terms of the [Creative Commons Attribution-NonCommercial-NoDerivs](https://creativecommons.org/licenses/by-nc-nd/4.0/) License, which permits use and distribution in any medium, provided the original work is properly cited, the use is non-commercial and no modifications or adaptations are made.

© 2024 The Authors. *Lasers in Surgery and Medicine* published by Wiley Periodicals LLC.

INTRODUCTION

Psoriasis is a chronic inflammatory skin disease characterized by erythrosquamous plaques, which affects 1%–5% of the population in the Western world.¹ The condition has a pronounced effect on the quality of life of patients, both due to the often accompanying pruritus² as well as the psychological–emotional burden from the actual or perceived risk of rejection by others.³ Treatment strategies typically consist of topical or systemic administration of drugs, such as corticosteroids, methotrexate, biologic agents, and calcineurin inhibitors. These strategies require continuous treatment, constituting a substantial burden on patients and healthcare systems. Moreover, while there is some evidence that these drugs aid in the clearing of psoriatic lesions,^{4,5} there are also indications of limited efficacy and side effects.^{6,7} Alternatively, narrow band 311 nm ultraviolet-B (UV-B) light therapy has been found to alleviate symptoms of severely affected psoriasis patients.⁸ Despite its significant disease-modifying potential,⁹ this approach, however, potentially carries a risk of inducing skin cancers.^{10–12} Earlier experience with laser therapy¹³ and dermatome shaving¹⁴ suggest that NB-UVB is not the only physical modality that can achieve durations of remission that are indicative of disease modification, for example, another light-based technique, the use of pulsed dye lasers (PDL) at visible wavelengths between 577 and 595 nm, offers the promise of long-term remission (one to multiple years) while causing little or no side-effects,^{13,15,16} by exploiting the process of selective photothermolysis (SPL).¹⁷

SPL comprises the targeted heating of blood vessels by means of the photo-thermal effect.¹⁸ Here, specific target molecules (chromophores) absorb radiant energy (light) and convert it to thermal energy (heat). Selecting chromophores (by tuning the wavelength of the light) that are located exclusively inside blood vessels (e.g., hemoglobin, the main constituent of red blood cells) then allows targeted heating of vascular structures. Moreover, through the subsequent dissipation of this heat, SPL can also affect some perivascular regions (depending on the laser pulse duration, vessel size, and location).¹⁹ In addition to direct effects of heating, such as coagulation or rupture of blood vessels, SPL can also induce secondary effects which may include suspending several of the processes that characterize psoriasis, such as angiogenesis,²⁰ inflammatory cytokine production,²¹ leukocyte-infiltration via endothelial adhesion molecules,²² and keratinocyte proliferation.²³ Furthermore, SPL may reduce the peripheral nerve fiber density and secretion of neuropeptides, which are both known to regulate the pathogenesis of psoriatic lesions.²⁴ It is not yet known which (combination) of these potentially SPL-arrested processes achieves local disease modification in psoriatic lesions, which currently stymies the creation of patient-tailored PDL-treatment protocols. Consequently, clinicians urgently require an improved understanding of

the underlying physiology of the remedial process, to provide optimal care to each patient (i.e., achieving long-lasting remission of psoriatic lesions using few treatments).

Unraveling how PDL treatment achieves long-term remission of psoriatic plaques requires the identification of pathogenic agents and processes most likely affected by it. Toward this goal, estimates of the physical effects of SPL in psoriatic lesions (i.e., light distribution and resulting temperature increase throughout the tissue as a function of space and time) should be used in conjunction with a priori knowledge about the immunopathology^{25–27} (i.e., location and heat sensitivity of pathogenic agents) to determine for which pathogenic processes these conditions may be critical (e.g., by effecting ablation of skin-resident immune cells, protein denaturation,^{28,29} or activation of heat-sensitive ion channels³⁰) and therefore warrant further lab-based investigation. We will refer to the associated temperatures as critical temperatures in the remainder of the manuscript.

Providing realistic estimates of these PDL-induced physical effects requires spatiotemporal modeling of the light propagation and subsequent photothermal heating within a psoriatic lesion. As a result of the geometric complexity and inter-personal variation of the model domain (i.e., the psoriatic lesion), no closed form analytical model exists for this purpose. Consequently, numerical solutions to the governing light and heat transport equations are required, rendering Monte Carlo modeling or the finite element method (FEM) suitable approaches.

While Monte Carlo modeling is a conceptually straightforward method to model light transport in turbid media, its application within complex geometric domains has long been challenging. Recently, however, substantial gains in the achievable model complexities (albeit on a larger length scale than the one studied here) as well as in the achievable computation speeds have been made.³¹ Notwithstanding, the finite element method provides some advantages for example, simultaneous solution of coupled multiphysics problems such as the one discussed in this paper. Moreover, the finite element method can be combined with adaptive mesh refinement and moving mesh techniques used to reduce numerical errors and model geometries undergoing time-dependent deformations, respectively.

In this study, we therefore use FEM in conjunction with an image-derived lesion morphology to provide, for the first time, realistic estimates of the PDL-induced physical effects within a psoriatic lesion. By solving both the transient photon diffusion and heat equations simultaneously, we compute the local photon density (and thereby the absorbed radiant energy) and the subsequent generation and dissipation of heat within a psoriatic lesion. We study the resulting spatiotemporal temperature field as a function of the (i) lesion

morphology (depth and distance from vascular structures of the heated locations) and (ii) laser wavelength (by adjusting the optical properties of optically active lesion constituents).

MATERIALS AND METHODS

Psoriatic lesion morphology used for the FEM calculations

To generate a FEM geometry closely resembling the lesion morphology (i.e., size, shape, and distribution of blood vessels), we used a confocal microscopy image of a fluorescently labeled section of a psoriatic skin specimen. To this end, a 3 mm punch biopsy was taken from a psoriatic lesion (under local sedation) of a patient with psoriasis vulgaris. The biopsy was obtained as part of a parallel MEC-approved clinical study which allowed for subsequent scientific use of the collected tissue material (MEC-U Medical Ethical Committee, METC, MEC-U, R20.10, NL75576.100.20, NCT05079256). The biopsy was fixed for 24 h in Zamboni fixative, washed twice in Sorrenson's buffer (0.1 M, Na_2HPO_4 , KH_2PO_4 , pH 7.6 at 4°C) for 5 min and stored at 4°C in a 20% glycerol buffer (20% glycerol, 20% Sorrenson's, 60% MilliQ). Then, the biopsy was embedded in TissueTek (Sakura Finetek USA Inc.) and sectioned at 80 μm with a Cryostat (Cryostat Cryostar NX70, Thermo Fischer Scientific Inc.). Individual sections were submerged in 30% antifreeze buffer (Ethylene Glycol, MilliQ) at -20°C until they were used. The staining protocol consisted of a

10 min wash in phosphate-buffered saline (PBS), followed by a 2 h blocking step in 4% normal goat serum and 0.1% Triton X-100 (Sigma Aldrich) in PBS to permeabilize the tissue. Next, the sections were incubated with 1:500 mouse anti-human CD31 conjugated to Alexa Fluor 647 dye (561654, BD Pharmingen) and 1:300 rabbit anti-human PGP9.5 (ab108986, Abcam) in a 1:1 ratio of PBS and blocking solution overnight at 4°C. Sections were rinsed twice in PBS for 5 min, and then incubated with 1:500 Cy3-goat anti-rabbit (111-165-144, Jackson ImmunoResearch Europe Ltd) for 2 h on a mild shaker at room temperature. Then, slides were rinsed in MilliQ to remove salt crystals and mounted in DAPI-containing Vectashield (Vector Laboratories Inc.). These slides were then imaged using a confocal fluorescence microscope (SP8-X DLS, Leica Camera AG), equipped with a $\times 40/1.3$ oil objective, using a 0.5 μm z-step size and 10% tile overlap. The left panel in Figure 1 shows such a confocal fluorescence microscopy image (of the endothelial staining) of a section of the psoriatic lesion biopsy. These images were segmented into a model geometry (consisting of blood vessels, dermis, and epidermis) using a custom-written, fully automated script (MATLAB 2020a, The MathWorks Inc.). The script comprises the following steps. As a first step, the 8-bit gray-scale confocal fluorescence microscopy image (of the endothelial staining) is loaded. Next, to facilitate segmentation of the blood vessels, the background (in this case the dermis and epidermis) is removed by a thresholding operation, followed by the application of a median filter to remove noise. The resulting image is then binarized using locally adaptive thresholding, where a threshold is

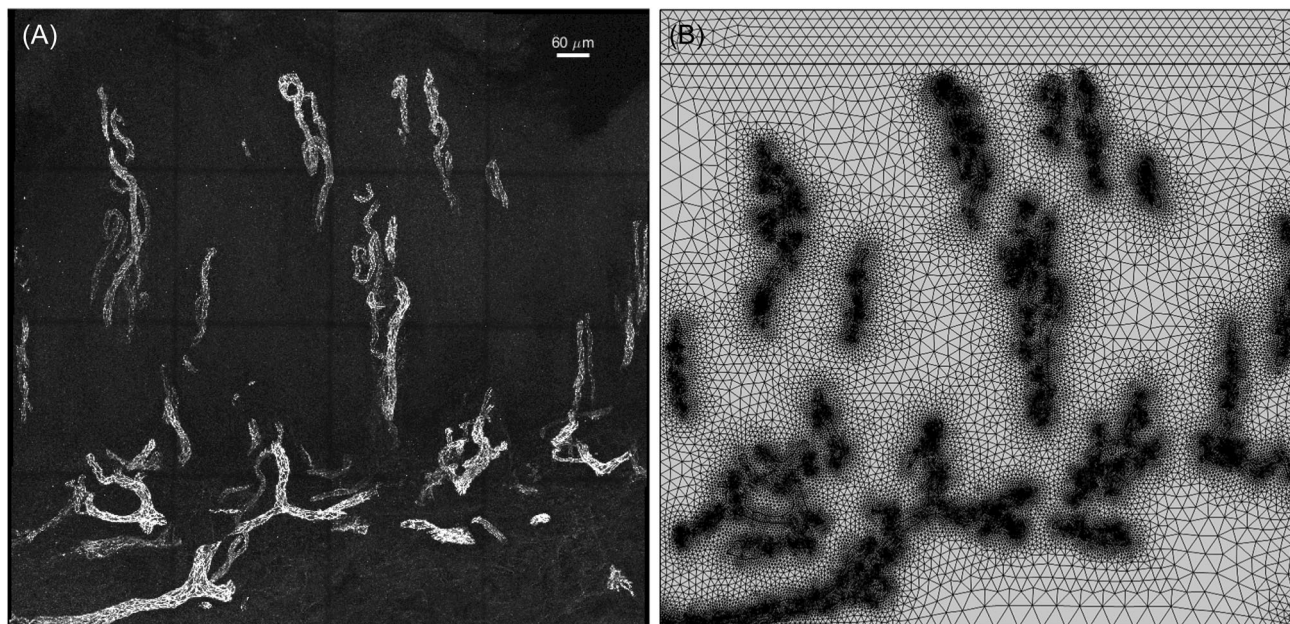


FIGURE 1 Psoriatic lesion morphology used for the finite element method calculations. Confocal fluorescence microscopy image of a psoriatic lesion biopsy, fluorescently labeled using the endothelial marker CD31 conjugated to Alexa Fluor 647 dye (left). Triangular mesh generated from the confocal fluorescence microscopy image consisting of 87,518 elements (right).

computed for each pixel using the local mean intensity around the pixel in a neighborhood approximately one-eighth of the size of the image.³² Next, the script detects all connected components (8-connectivity) within this binarized image. This is followed by a flood fill operation to fill small holes in the blood vessels resulting from the endothelial staining. A Moore-Neighbor tracing algorithm (in conjunction with Jacob's stopping criteria)³³ is then used to trace the inner (in the case of loops) and outer boundaries of the segmented blood vessels. This step is necessary to correctly recognize the areas within vascular loops as dermal tissue. The epidermis is added as a layer of pixels at the top of the image in accordance with the epidermal thickness determined in the microscopy image. Finally, the resulting segmented image (comprising multiple regions of three distinct tissue types, namely epidermis, dermis, and blood vessels) is then discretized into a triangular mesh (such as the one shown in the right panel of Figure 1) using an open-source MATLAB toolbox.³⁴ This triangular mesh is then loaded into the FEM software and used as a model geometry.

Light-transport modeling

To predict the light distribution throughout the psoriatic lesion as a result of the pulsed laser irradiation, we employ the time-dependent diffusion equation³⁵:

$$\frac{\partial}{\partial t} \phi(x, z, t) - \nabla D_i \nabla \phi(x, z, t) = -c_i \mu_{a,i} \phi(x, z, t),$$

where

$$D_i = \frac{c_i}{3[\mu_{a,i} + (1 - g_i)\mu_{s,i}]}.$$

Here, $\phi(x, z, t)$ denotes the photon fluence rate and carries the unit $\text{m}^{-2}\text{s}^{-1}$, D_i is the optical diffusion coefficient of tissue region i (i.e., e = epidermis, d = dermis, b = blood vessel) and carries the unit m^2s^{-1} , $\mu_{a,i}$ and $\mu_{s,i}$ represent the absorption and scattering coefficient of tissue region i and carry the unit m^{-1} , g_i is the dimensionless optical anisotropy factor of tissue region i , and c_i is the speed of light in tissue region i and carries the unit ms^{-1} . The values of these optical properties used in this study (i.e., at 585 and 595 nm) are listed in Tables 1 and 2. Most clinically used PDL devices (e.g., the Candela V-beam and DEKA Synchro VasQ or their predecessors) operate at these two wavelengths. We model the incident laser pulse as a photon flux across the skin-air boundary using the following boundary condition:

TABLE 1 Optical properties of the different tissue regions at 585 nm.

Tissue region	μ_a (m^{-1})	μ_s (m^{-1})	n (-)	g (-)
Blood	19,100	46,700	1.33	0.995
Dermis	24	12,900	1.37	0.79
Epidermis	1800	47,000	1.37	0.79

Note: Optical properties correspond to a Fitzpatrick skin type 2 with 6% melanosomes.^{36,37}

TABLE 2 Optical properties of the different tissue regions at 595 nm.

Tissue region	μ_a (m^{-1})	μ_s (m^{-1})	n (-)	g (-)
Blood	4930	46,600	1.33	0.995
Dermis	24.5	12,000	1.37	0.8
Epidermis	1550	48,000	1.37	0.8

Note: Optical properties correspond to a Fitzpatrick skin type 2 with 6% melanosomes.^{36,37}

$$\frac{c(1-R)P(t)}{E_p} = -D_e \nabla \phi(x, z, t).$$

Here, $P(t)$ denotes the temporal profile of the laser pulse irradiance incident on the tissue as a function of the pulse time and carries the unit Wm^{-2} , R is a dimensionless reflection factor measuring the fraction of the laser light that is reflected by the lesion surface, c is the speed of light in vacuum, and E_p represents the energy of a single photon at the chosen wavelength and carries the unit J. Here, we model $P(t)$ as a single, continuous 0.45 ms pulse with a radiant exposure of 8Jcm^{-2} . The pulse duration is in accordance with current clinical practice in laser therapy for psoriasis vulgaris. Finally, to virtually extend the tissue beyond the model geometry we employ the following boundary condition at the tissue-tissue boundary:

$$c_i \phi(x, z, t) = -D_i \nabla \phi(x, z, t).$$

Heat-transport modeling

To compute the generated temperature field throughout the lesion as a function of space and time, we numerically solve the heat equation, where the absorbed light distribution predicted by the diffusion equation serves as the source term:

$$\rho_i C_i \frac{\partial T(x, z, t)}{\partial t} - \nabla k_i \nabla T(x, z, t) = \rho_i C_i u_p (T_b - T(x, z, t)) + \mu_{a,i} \phi(x, z, t) E_p E_{f,i}.$$

TABLE 3 Thermal properties of the different tissue regions.

Tissue region	k (W m ⁻¹ K ⁻¹)	ρ (kg m ⁻³)	C_p (J kg ⁻¹ C ⁻¹)
Blood	0.55	1100	3600
Dermis	0.53	1200	3800
Epidermis	0.21	1200	3600

Here, $\mu_{a,i}\phi(x, z, t)E_p E_{f,i}$ denotes the heat source resulting from the absorption of radiant energy by the chromophores of the different tissues and carries the unit W m⁻³; $E_{f,i}$ refers to the volume fraction of the chromophores, for example, 0.45–0.25 for hemoglobin (depending on the hematocrit of different vessel types) and 0.16–0.04 for melanin (depending on the skin type); $T(x, z, t)$ represents the spatial temperature field as a function of time; ρ_i denotes the density of the tissue region i and carries the unit kg m⁻³; k_i refers to the thermal conductivity of tissue region i and carries the unit W m⁻¹ K⁻¹; u_p is a mass transport coefficient with the unit 0.028 kg m⁻³ s⁻¹ and accounts for heat transport through perfusion³⁸; T_b is the core body temperature at $t=0$; and C_i refers to the specific heat capacity of tissue region i with unit J kg⁻¹ °C⁻¹.

We model the initial spatial temperature distribution as 37°C everywhere except at the air-tissue boundary (the skin) where the initial temperature is set to 26°C, that is, $T(z > 0) = 37^\circ\text{C}$ and $T(z = 0) = 26^\circ\text{C}$. Convective heat transport at the lesion surface is modeled as

$$-k\nabla T = h_s(T - T_{\text{amb}}).$$

Here, the convective heat transfer coefficient h_s was set to 150 W °C⁻¹ m⁻² in accordance with the value for free convection across a flat plate³⁹ outside the irradiated zone, where $T_{\text{amb}} = 26^\circ\text{C}$. Similarly, we describe perfusion-mediated transport of heat at the intralesional boundaries (i.e., the sides) of the modeled geometry as

$$-k\nabla T = u\rho_i C_i(T_b - T),$$

where u is the bulk blood flow velocity taken as 0.0003 m s⁻¹.⁴⁰ The values of all thermal properties used for the simulations in this study are listed in Table 3.

Evaluation of the resulting intralesional temperature field

To evaluate the spatiotemporal characteristics of the resulting temperature field we numerically solved the transient diffusion and the transient heat equation simultaneously, subject to their respective boundary conditions, within the image-derived, discretized domain

(COMSOL Multiphysics[®] v. 5.4, COMSOL AB). The predicted temperatures were saved at all mesh nodes, for times ranging from 0 to 1 s, where the saved timepoints were separated by 1 μs intervals from the beginning until the end of the laser pulse (i.e., for $0 \leq t \leq 0.45$ ms) and by 1 ms intervals thereafter (i.e., for $0.45 \text{ ms} < t \leq 1$ s).

As a first step we selected only intervascular and vessel wall locations for further analysis, yielding two types of locations in total, which we refer to as *tissue* and *epithelium* in the remainder of this manuscript. We then determined whether the predicted temperatures of the selected locations exceeded any of four given critical temperatures (43°C, 52°C, 60°C, and 70°C), at any point in time and if so, noted the maximum temperature reached at these locations. These four critical temperatures are associated with the activation of cellular ion channels^{41,42} (43°C and 52°C), neuronal cell death (60°C), and vascular coagulation⁴³ (70°C), respectively. Next, we computed the consecutive (i.e., continuous) duration of the temperature exceeding any critical temperature. Finally, we determined the location's smallest Euclidian distance to any vessel wall (which is zero for the epithelial locations) as well as its depth as measured from the skin surface.

RESULTS

Figure 2 shows the computed spatial temperature field following a 0.45 ms continuous laser pulse at 585 nm (left) and 595 nm (right) and 8 J cm⁻² radiant exposure. Here, the irradiated epidermis reaches a maximum temperature of 46.3°C in both cases. The intra-vascular temperature exhibits a spatial dependence, with higher temperatures at the top and lower temperatures at the bottom (with respect to the skin surface).

Figure 3 comprises boxplots of the following metrics for locations at which the predicted temperature exceeds any of the five critical temperatures at any point in time (for a laser wavelength of 585 nm): (i) the *consecutive* duration of temperatures exceeding the critical temperatures, (ii) the depth of these locations (as measured from the skin surface), (iii) the maximum temperature reached at these locations, and (iv) the distance from any vessel wall at these locations (which is zero for the vascular epithelium). The results are divided into two categories according to their location within the lesion, namely: between separate blood vessels (denoted as *Tissue*, panels A–D) or within a vessel wall (denoted as *Epithelium*, panels E–G), and presented as a function of the critical temperature. Figure 4 shows the same metrics for a laser wavelength of 595 nm.

For both location categories (i.e., *Tissue* and *Epithelium*), the maximum temperatures reached at a laser wavelength of 585 nm exceed those reached at 595 nm (Figures 3C,G,4C,G). Of these, the overall maxima correspond to ~200°C and ~120°C at 585 and 595 nm,

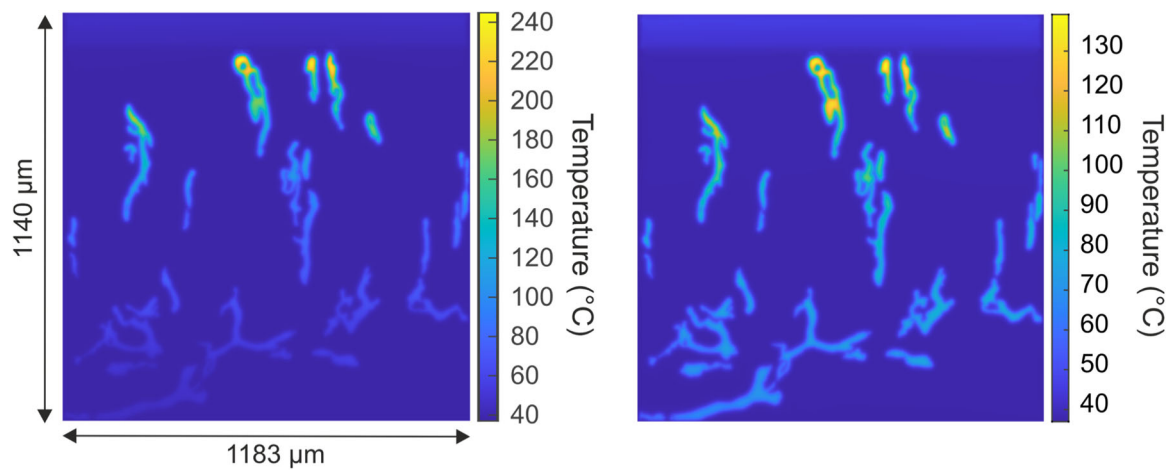


FIGURE 2 Temperature distribution. Generated temperature field at the end of a 0.45 ms continuous laser pulse at 585 nm (left) and at 595 nm (right) and incident radiant exposure of 8 J cm^{-2} . Note the difference in the temperature scale.

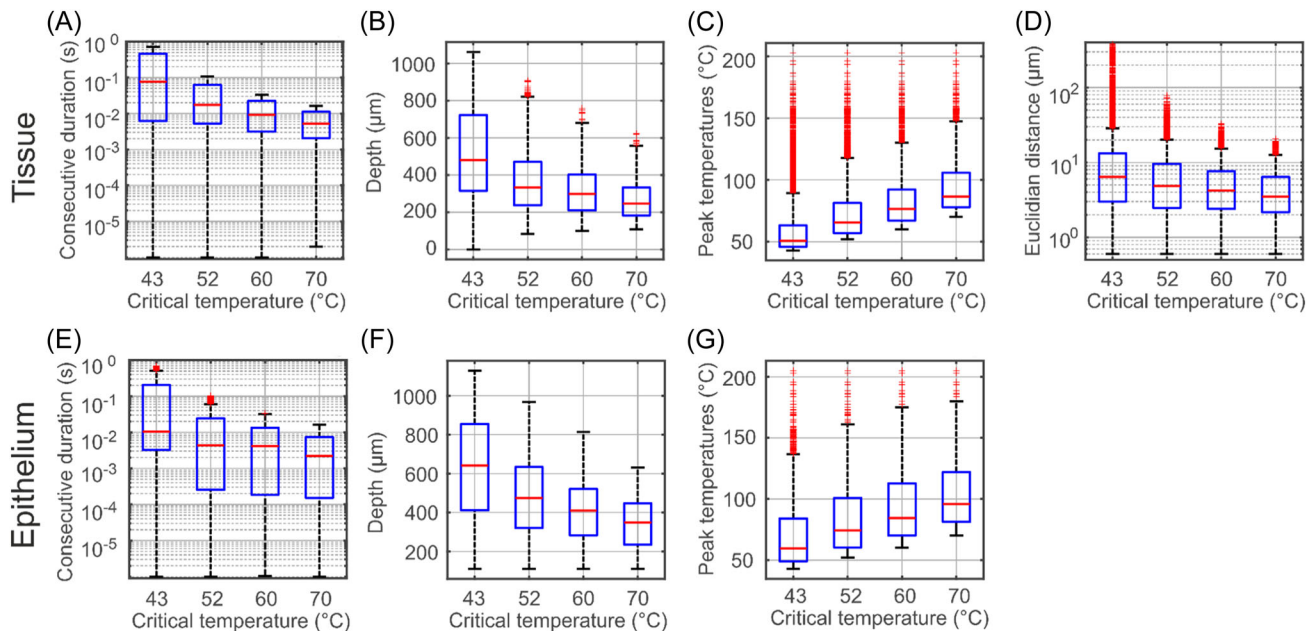


FIGURE 3 Heating characteristics of blood vessel-adjacent tissue and epithelial locations exceeding 43°C , 52°C , 60°C , and 70°C during (and up to 1 s after) a continuous 0.45 ms laser pulse at 585 nm and 8 J cm^{-2} . All characteristics are shown as a function of the critical temperature. *Tissue* and *Epithelium* refer to locations between blood vessels and the blood vessel walls, respectively. *Tissue*: (A) *Consecutive duration* of the period during which the temperature at these locations exceeds the critical temperatures. (B) *Depth* of locations whose temperature exceeds the critical temperature at any point in time. (C) *Peak temperatures* reached at locations whose temperature exceeds the critical temperature at any point in time. (D) *Distance* from any blood vessel wall of locations that exceed the critical temperature at any point in time. *Epithelium*: (E) *Consecutive duration* of the period during which the temperature at these locations exceeds the critical temperatures. (F) *Depth* of locations whose temperature exceeds the critical temperature at any point in time. (G) *Peak temperatures* reached at locations whose temperature exceeds the critical temperature at any point in time.

respectively. The upper quartiles of the peak temperature distributions for all critical temperatures exceed 50°C . Finally, the maximum temperatures for all locations increase with increasing critical temperature.

Conversely, the depth of the locations exceeding the critical temperatures decreases with increasing critical temperature for both laser wavelengths and location categories (Figures 3B,F,4B,F). Overall, larger depths are achieved at a laser wavelength of 595 nm (Figure 4B,F).

Here, maximum depths exceed $500 \mu\text{m}$ (median $225 \mu\text{m}$) for a critical temperature of 70°C and $1050 \mu\text{m}$ (median $625 \mu\text{m}$) for a critical temperature of 43°C for the *tissue* locations (Figure 4B) and $900 \mu\text{m}$ (median $300 \mu\text{m}$) for a critical temperature of 70°C and $1100 \mu\text{m}$ (median $750 \mu\text{m}$) for a critical temperature of 43°C for the *epithelial* locations (Figure 4F). At 585 nm, maximum depths exceed $600 \mu\text{m}$ (median $250 \mu\text{m}$) for a critical temperature of 70°C and $1050 \mu\text{m}$ (median $500 \mu\text{m}$) for a

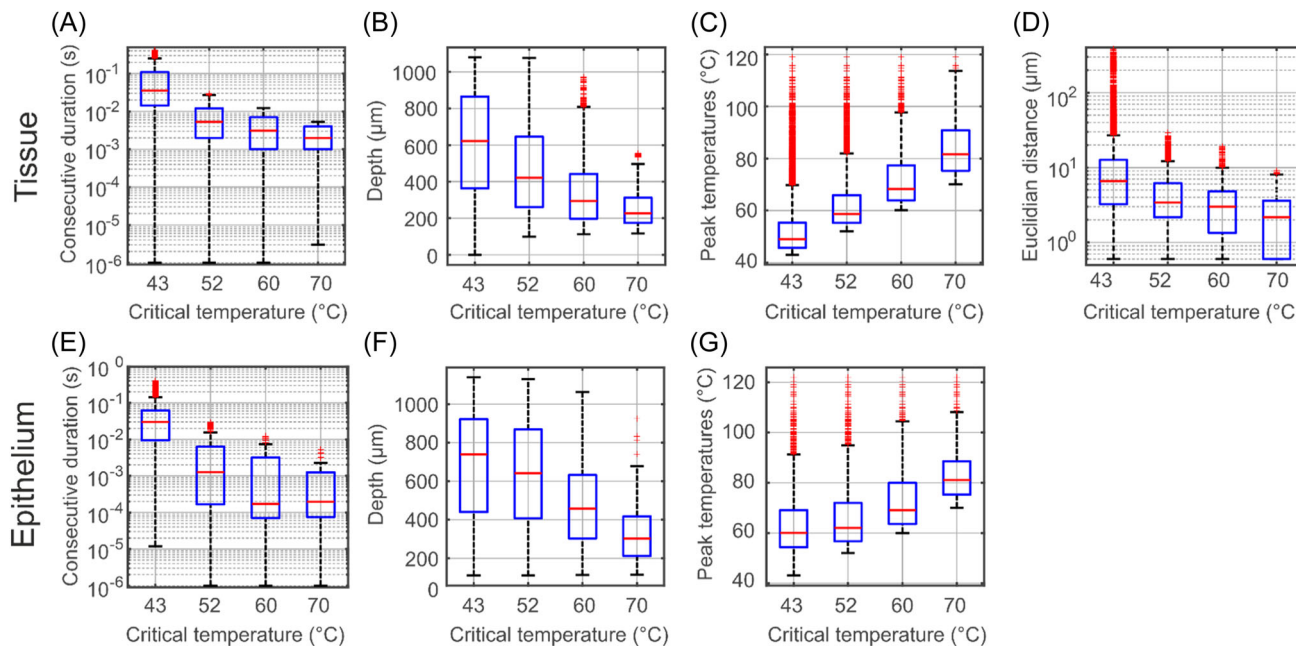


FIGURE 4 Heating characteristics of blood vessel-adjacent tissue and epithelial locations exceeding 43°C, 52°C, 60°C, and 70°C during (and up to 1 s after) a continuous 0.45 ms laser pulse at 595 nm and 8 J cm^{-2} . All characteristics are shown as a function of the critical temperature. *Tissue* and *Epithelium* refer to locations between blood vessels and the blood vessel walls, respectively. *Tissue*: (A) *Consecutive* duration of the period during which the temperature at these locations exceeds the critical temperatures. (B) Depth of locations whose temperature exceeds the critical temperature at any point in time. (C) Peak temperature reached at locations whose temperature exceeds the critical temperature at any point in time. (D) Distance from any blood vessel wall of locations that exceed the critical temperature at any point in time. *Epithelium*: (E) *Consecutive* duration of the period during which the temperature at these locations exceeds the critical temperatures. (F) Depth of locations whose temperature exceeds the critical temperature at any point in time. (G) Peak temperature reached at locations whose temperature exceeds the critical temperature at any point in time.

critical temperature of 43°C for the *tissue* locations (Figure 3B), and 600 μm (median 350 μm) for a critical temperature of 70°C and 1100 μm (median 625 μm) for a critical temperature of 43°C for the *epithelial* locations (Figure 3F). The upper quartiles of all depth distributions exceed 300 μm for both wavelengths (Figures 3B,F,4B,F).

The distances from any vessel wall for *tissue* locations exceeding the critical temperatures exhibit a similar trend as the depth data by decreasing with increasing critical temperature (Figures 3D and 4D). At 595 nm, maximum distances of $\sim 350 \mu\text{m}$ (median 7 μm) and $\sim 10 \mu\text{m}$ (median 2 μm) are achieved at tissue locations for critical temperatures of 43°C and 70°C, respectively (Figure 4D). For a laser wavelength of 585 nm and critical temperatures of 43°C and 70°C, the maximum distances achieved at tissue locations correspond to $\sim 350 \mu\text{m}$ (median 7 μm) and $\sim 20 \mu\text{m}$ (median 4 μm), respectively (Figure 3D).

The consecutive duration for which the temperatures at a given location exceed the critical temperatures also decreases with increasing critical temperature (for both tested laser wavelengths, Figures 3A,E,4A,E). At 595 nm, the maximum consecutive durations of temperatures exceeding 43°C and 70°C (at *tissue* locations) correspond to $\sim 400 \text{ ms}$ (median 40 ms) and 5 ms (median 2 ms), respectively (Figure 4A), and (for *epithelial* locations) to $\sim 500 \text{ ms}$ (median 30 ms) and 6 ms (median 0.2 ms),

respectively (Figure 4E). Overall, the consecutive durations achieved at 585 nm exceed those achieved at 595 nm, with all upper quartiles exceeding 5 ms (Figure 3A). At *tissue* locations with temperatures exceeding 43°C and 70°C, maximum achieved consecutive durations correspond to $\sim 700 \text{ ms}$ (median 80 ms) and $\sim 15 \text{ ms}$ (median 5 ms), respectively (Figure 3A), and at *epithelial* locations to $\sim 800 \text{ ms}$ (median 10 ms) and $\sim 15 \text{ ms}$ (median 2 ms), respectively (Figure 3E).

Figures 5 and 6 show spatial maps of the consecutive durations for which the pre-set critical temperatures are sustained and the maximum temperatures reached at these locations at 585 nm (panels A–D) and 595 nm (panels E–H), respectively.

DISCUSSION

The main objective of this study is to provide estimates of PDL-induced photothermal effects within psoriatic lesions (for laser wavelengths of 585 and 595 nm), with the aim of identifying pathogenic processes likely affected by these conditions. To this end, we used FEM in conjunction with an image-derived psoriatic lesion morphology. First, we defined the model geometry by segmenting blood vessels from a confocal microscopy image of a fluorescently labeled section of a psoriatic skin

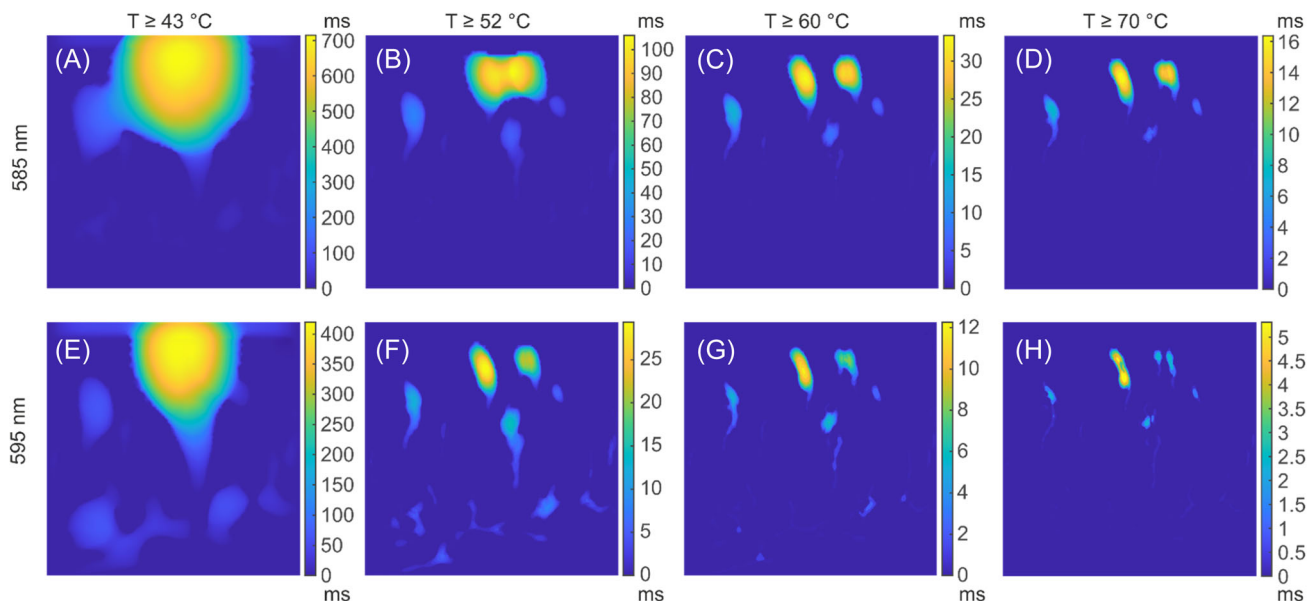


FIGURE 5 Spatial maps showing the consecutive durations for which the pre-set critical temperatures (columns) are sustained from the beginning of a 0.45 ms continuous laser pulse at 585 nm (panels A–D) and 595 nm (panels E–H) and an incident radiant exposure of 8 J cm^{-2} . Note the different color scales indicating the consecutive duration in ms.

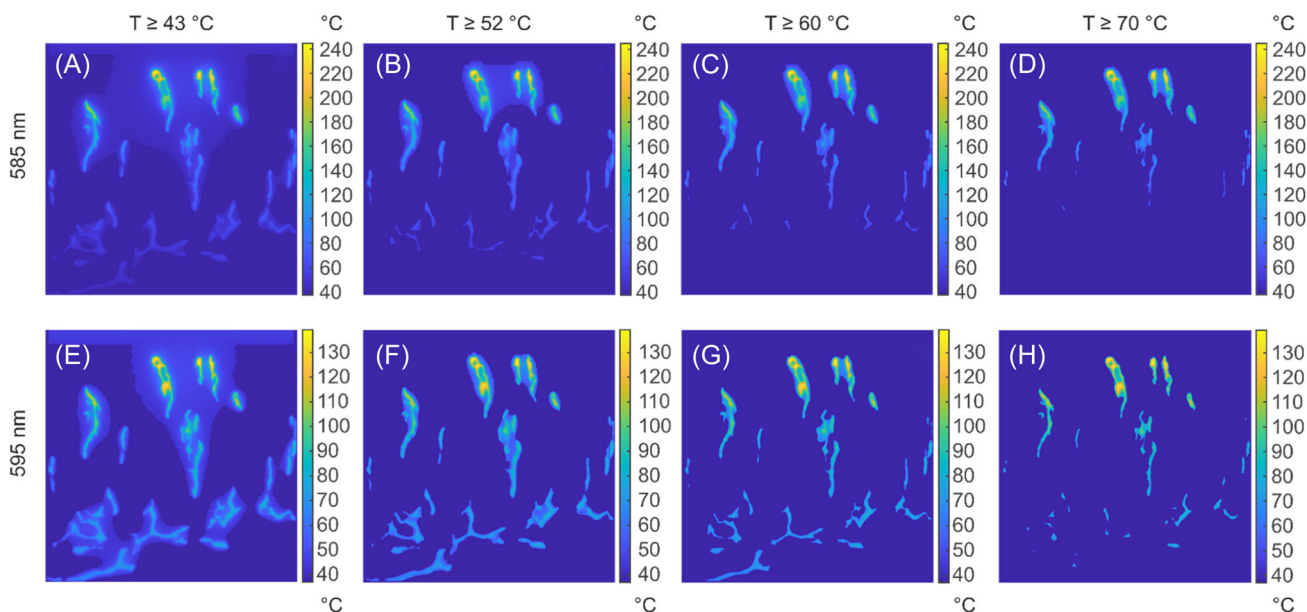


FIGURE 6 Spatial maps showing the maximum temperatures reached at the locations for which the pre-set critical temperatures (columns) are exceeded using a 0.45 ms continuous laser pulse at 585 nm (A–D) and 595 nm (E–H) and an incident radiant exposure of 8 J cm^{-2} . Note the different color scales indicating maximum temperatures in $^\circ\text{C}$.

specimen (see Figure 2). Next, we modeled the laser light propagation and subsequent photothermal heating by numerically solving the transient diffusion and heat equations simultaneously. The resulting high-resolution spatiotemporal predictions of the generated temperature field within the lesion, in turn, allowed computation of the following quantitative measures. Locations reaching pre-set critical temperatures were characterized in terms of (i) the consecutive duration of their exceeding the

critical temperatures, (ii) their depth (from the skin surface), (iii) their maximum temperature, and (iv) their distance from any blood vessel wall (see Figures 3–6).

The overall increased maximum temperatures and reduced penetration depths achieved at 585 nm correspond with the vastly increased absorption coefficient and slightly reduced scattering coefficient of blood at this wavelength. As a result of the higher intra-luminal and epithelial temperatures, critical temperatures are achieved

at greater distances from the blood vessels and sustained for longer consecutive durations.

The PDL-induced heating of blood vessels may play a role in the remission of psoriatic plaques in several ways. Photothermal changes to the local nerve structure and function have been suggested as a possible remedial pathway,⁴⁴ following observations of denervation causing a spontaneous remission of psoriatic lesions.⁴⁵ These changes may comprise direct and indirect forms of nerve damage, such as thermal denaturation of the perivascular nerves or a depletion of the molecular microenvironment through compromised vascular functionality, respectively. In the following, we discuss these direct and indirect changes and their potential association with the PDL-induced photothermal effects in more detail.

Thermal nerve damage

Thermal damage to nerves may occur through neuronal denaturation upon heat dissipation from the nearby blood vessels. In a study from our lab (which will be presented in a forthcoming manuscript "Sub-minute thermal damage to cell types present in the skin"), we observed that neuronal cell viability is substantially reduced at a critical temperature of 60°C. Perivascular nerves can be found in close proximity (on the order of micrometers) of the blood vessel walls^{46,47} (also substantiated by a fluorescently labeled biopsy section shown in Figure 7). Our simulations predict that almost all locations that reach 60°C are within 18 μm (at 585 nm) and 11 μm (at 595 nm) of a blood vessel wall, indicating that neuronal cell viability of perivascular nerves may be affected by PDL treatment. Free sensory nerves, however, can also be found at much larger distances, where they are less likely to be affected by the vascular heat dissipation.

A second pathway by which nerves may experience PDL-induced thermal damage is mediated by two heat-sensitive transient receptor potential vanilloid (TRPV) channels, namely TRPV1 and TRPV2. These channels are present on neuronal and immune cells to regulate the cellular influx of Ca²⁺ ions and the release of inflammatory cytokines. TRPV1 and TRPV2 activate (open) at 43°C and 52°C, respectively. Extended activation of these channels may cause cytoplasmic calcium concentrations to reach non-physiological levels, in turn, inducing cell swelling and neuronal death.⁴⁸ Furthermore, it has been found that TRPV1 is upregulated in pruritic psoriatic lesions⁴⁹ and that topical application of capsaicin, a molecular agonist (activator) of TRPV1, achieved reduction in psoriatic lesion severity and inflammation,⁵⁰ substantiating the role of TRPV1 in psoriasis remission. In our computations, a critical temperature of 43°C is generated at locations within up to 140 μm of a vessel wall (at both wavelengths) and

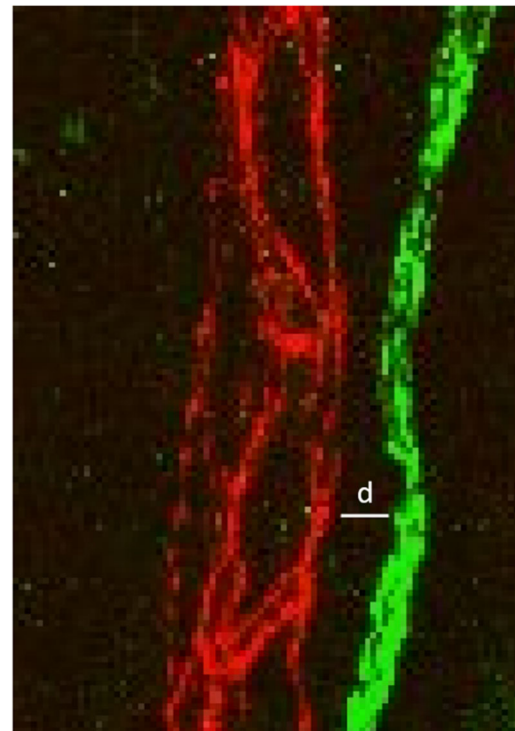


FIGURE 7 Section of a confocal microscopy image of a 3 mm punch biopsy of a psoriatic lesion. The red pixels depict a blood vessel (labeled via the endothelial marker CD31) and the green pixels indicate a perivascular nerve (labeled via the peripheral nerve marker PGP9.5). The distance indicated by the line d equals 5.4 μm.

sustained for up to 0.7 s (at 585 nm) and 0.4 s (at 595 nm), while a critical temperature 52°C is reached by locations within 20 μm (at 585 nm) and 13 μm (at 595 nm) of a vessel wall and sustained for up to 130 ms (at 585 nm) and 23 ms (at 595 nm). These results render activation of TRPV1 and TRPV2 channels in perivascular nerves and immune cells highly likely (further substantiated by the pain sensation experienced by many patients treated with PDLs^{51,52}). It has yet to be determined, however, what the extent of the induced channel opening would be (given these temperatures and activation times) and whether it is sufficient to induce cytotoxic Ca²⁺ levels. Furthermore, there is experimental evidence that TRPV1 channels can be thermally irreversibly inactivated,⁵³ potentially inhibiting this pathogenic pathway. A forthcoming study from our lab will therefore characterize the heat sensitivity of several cell types (neuronal cells, keratinocytes, endothelial cells, and smooth muscle cells) associated with various suspected therapeutic and pathogenic pathways (e.g., neurogenic inflammation, angiogenesis, partial or total loss of vascular functionality), which in conjunction with the results of the present study may yield new insights on the remedial mechanisms of the laser-based treatment of psoriatic lesions.

Compromised vascular functionality

Coagulation of blood vessels may lead to compromised blood vessel functionality, resulting in local hypoxia, depletion of nutrients, waste accumulation, and changes in the extracellular matrix.^{54–56} By creating such an unfavorable environment⁵⁷ for nerve regeneration and angiogenesis, compromised vascular functionality may therefore extend the remission period. Similarly, a partial or total loss of the functionality of blood vessels may stall infiltration of activated T cells, which are suspected to mediate plaque formation by the release of growth factors and inflammatory cytokines.⁵⁸ Our results indicate that the coagulation-inducing⁴³ temperature of 70°C is sustained in the vascular epithelium for up to 19 and 5 ms at 585 and 595 nm, respectively. Whether these time scales are sufficient to induce vessel wall coagulation has yet to be determined experimentally. However, our predictions of the maximum and mean depths at which a temperature of 70°C is reached in the vascular epithelium (at 585 nm irradiation), namely 620 μm and (348 \pm 127) μm , respectively, are in excellent agreement with a previous experimental study, which found that the overall vessel-wall coagulation depth was limited to a maximum of 650 μm (mean 370 μm).⁵⁹ The same study also found complete coagulation of vessels smaller than 150 μm in diameter for the laser settings used in our simulations, rendering at least a partial reduction in vascular functionality of the small vessels studied here possible. Note that while these are compelling similarities, our findings are based on a single biopsy and some variation in these measures is possible between lesions and donors. Moreover, all quantitative measures investigated in this study depend on the specific spatial configuration of the blood vessels, as can be seen in Figures 5 and 6. Here, temperatures and consecutive durations in the intervascular space between four superficial blood vessels at 585 nm (three at 595 nm) exceed those on either side of the grouping. This is a result of the intervascular distance matching the length scale of the heat diffusion from the surrounding blood vessels, thereby achieving an additive effect. Consequently, high-resolution *in vivo* imaging of blood vessels will likely be necessary for the creation of maximally individualized treatment protocols. Similarly, using our approach to investigate treatment effectiveness would require noninvasive tomographic *in vivo* imaging techniques (e.g., optical coherence tomography⁶⁰ or photoacoustic imaging⁶¹) to be able to assess the tissue before and after treatment.

Notwithstanding that the approach developed in this study constitutes a significant advance in our ability to study the therapeutic mechanisms of photothermal treatments of a variety of tissue pathologies in a patient-tailored manner, there is scope to further extend the technique's applicability and usefulness to answer relevant biological questions. Moreover, to unravel the

remedial process of laser-based treatments of psoriatic lesions, the pathogenic processes identified in this work as likely affected by the laser-induced photothermal effects should be the focus of future experimental studies.

First, our computational approach currently utilizes constant values for the optical and thermal properties of the different tissue regions. These, however, are most likely temperature-dependent.^{62–64} While these dependencies are easily implemented computationally, their exact form is subject of some debate and notoriously difficult to determine experimentally (particularly *in vivo*).⁶⁵ Accordingly, there is an urgent need for the development of novel methods which allow rigorous experimental characterization of these properties (ideally *in vivo*). Second, arguably, the assumption of spatially uniform bulk optical properties within the blood vessels in our model may not be valid, since at our model scale the diameters of the blood vessels and their enclosed erythrocytes become comparable. Again, while resolving this issue computationally is relatively simple, the lack of non-bulk optical properties (e.g., of individual erythrocytes) renders this solution challenging. Similarly, we currently do not model several tissue constituents of interest explicitly (e.g., vascular epithelium, nerves fibers). While the addition of such tissue constituents as separate model domains may increase the accuracy of our computations, their relative size with respect to the entire model domain would vastly increase the required number of finite elements and hence the computational cost. Moreover, including these tissue constituents in the heat transfer calculations necessitates knowledge of their thermal properties, which, much like the optical properties, are difficult to determine experimentally, particularly *in vivo*. Third, in this study, we numerically solve the diffusion approximation to the radiative transfer equation to model the photon distribution within the tissue. As a result, the fluence rate in highly light-absorbing regions such as the blood vessels may be underestimated. Since in this study, however, the physical dimensions of these regions are on the order of a few mean free paths, the effect of this underestimation is arguably not substantial.⁶⁶ For geometries containing large absorbing regions, the radiative transfer equation can be solved directly in a FEM environment using the discrete ordinates methods,^{67–69} at a significantly increased computational cost.

Fourth, in this study, we used a fluorescently labeled, fixed tissue section to define our model geometry. It is, therefore, conceivable that the imaged tissue section was subject to shrinkage, incurring inaccuracies in the physical extent of the model domain. This, in turn, would impact the amount of absorbed light and hence generated heat, as well as the computed quantitative measures. Similarly, since the biopsy sections were not fixed at physiological pressures, it is possible that the imaged blood vessel diameters are smaller than their *in vivo* diameters. Simulations carried out for 1.7-fold

increased blood vessel diameters, however, showed no substantial effect on the temperature distribution (data not shown). Fifth, our approach currently employs a static model geometry. The heat-induced structural changes (e.g., collagen denaturation, blood vessel coagulation, increase in interstitial fluid volume fraction, thermal tissue expansion, liquid evaporation), however, may correspond to a dynamic tissue morphology. Such effects can be modeled using moving meshes and adaptive finite element methods,⁷⁰ again at an increased computational cost. Likewise, our method does not explicitly model dynamic fluid flow. Such fluid flow may play a role in the heat transport in the form of convection. Furthermore, blood flowing out of the irradiation zone may result in a reduction in the locally generated heat by reducing the irradiation duration of the chromophores. While for the small blood vessels studied here blood flow velocities are sufficiently low to assume a static chromophore distribution, for morphologies comprising larger blood vessels the effects may not be negligible. In that case, computational fluid dynamics⁷¹ could be added to the existing framework, which would substantially increase the computational cost (particularly at this microscopic scale) and model complexity. Finally, we represent the thin tissue section computationally using a two-dimensional model geometry, which does not include light or heat diffusion in the third dimension, potentially yielding elevated temperatures. To overcome this limitation, future work will focus on an extension of our approach to larger three-dimensional geometries generated from stacks of consecutive sections.

In this study, we simulated the PDL-induced temperature change within a psoriatic lesion of Fitzpatrick skin type 2. We expect that all four quantitative measures considered in this study would be lower for darker skin types, as some of the incident radiation would already be absorbed in the more strongly pigmented epidermis (where reached peak temperatures would be higher compared with lighter skin types). Moreover, the location of the lesion and the corresponding epidermal thickness⁷² may affect the considered quantitative measures in a similar way by reducing the amount of light reaching the blood vessels for locations with increased epidermal thickness. Furthermore, the effect of varying density, tortuosity, and distribution of blood vessels at different body locations⁷³ may be two-fold. Hotspots like the one shown in Figures 5 and 6 require vessels in close proximity, that is, increased vascular tortuosity or denser vascular networks. Denser networks of superficial vessels, however, may also prevent heating of more deeply located vessels, creating a trade-off between achievable depths and inter-vascular distances of the heated perivascular regions. Finally, the age of the patient may affect a variety of factors, notably through a reduction in epidermal thickness for older patients⁷² (arguably increasing achievable depths of the heated

perivascular regions), but also in the collagen content and hydration state of the skin (which may affect the thermal properties of the skin, which, in turn, govern the heat transport) and potentially an impaired perfusive thermoregulatory response⁷⁴ (potentially increasing reached peak temperatures). Finally, we did not model active skin cooling, since the coagulation predictions were compared to results of a study that was performed without cooling. While cooling plays a key role in epidermal protection, it was not the focus of this study. Furthermore, the analyses were done for Fitzpatrick skin type 2 at moderate radiant exposures, where forced cooling is less critical.

Another subject of debate is the governing equation used to model the heat transport within the tissue. As this governing equation is a parabolic partial differential equation, it inherently propagates information at infinite speeds.⁷⁵ Physicists refer to this phenomenon as *instantaneous action*, that is, energetic changes at one location within the model domain are felt immediately (instantaneously) at all other points, implying an infinite (unphysical) speed of propagation. Researchers in the 1950s suggested to remedy this paradox by enforcing a temporal delay (often referred to as a “phase lag” or “thermal relaxation time”) in the heat flux (at a given location) with respect to the spatial temperature gradient (at that location).^{76,77} Experimentally determined phase lags (relaxation times) of specific tissues, however, still vary greatly among studies, necessitating more rigorous experimental characterization of this phenomenon within different tissue types.⁷⁸

Thermal tissue damage is most commonly predicted with a quantitative measure referred to as the Arrhenius damage integral.⁷⁹ In its differential form, this integral can easily be solved simultaneously alongside the transient light and heat transport equations using our approach. This relationship, however, is based on an empirical observation in gases and the required tissue-specific parameters (the frequency factor A and the activation energy barrier E_a) are subject to substantial variability (several orders of magnitude) among literature sources. Moreover, the mathematical models designed to predict thermal tissue damage necessarily have to rely on simplifying assumptions in their description of the complex biochemical heat response of human tissue. Furthermore, not all aspects of the biochemical response are fully understood yet. Consequently, the modeling of thermal tissue damage as a function of critical temperatures and exposure times (consecutive durations) remains challenging and the subject of continued debate.^{28,80–83} This, in turn, underscores the need for comprehensive experimental datasets of the underlying processes to aid in the development and improvement of these damage models.

While severe cases of psoriasis can benefit from biologic agents and comparable interventions, patients suffering from limited forms of the disease, however, are

not so fortunate. As a result, PDL is still being used for specialized indications (e.g., nail psoriasis⁸⁴) and treatment-resistant common plaques frequently located at the hands, feet, elbows, and knees.⁸⁵ Furthermore, based on clinical experience (which researchers involved in this study gained while treating more than 950 psoriasis patients), it seems that particularly patients suffering from itch benefit from PDL, as the effect of laser therapy on itch occurs in one or two treatments, long before the erythema and induration decreases. Finally, the poor correlation between disease severity and the impact of psoriasis on the quality of life implies that there is a large group of patients with unmet needs (also suggested by the literature on patients' perspective^{86,87}). Consequently, for a vulnerable minority the need to better understand this treatment is pivotal, as an improved understanding of how the treatment achieves both clearance and long-term treatment free remission will allow patient-tailored treatment protocols (and hence reduce the number of required treatments). This, in turn, means that more people can be helped in a shorter timeframe.

CONCLUSION

We demonstrated that FEM in conjunction with image-derived morphologies allows simultaneous computation of laser light propagation and the resulting photothermal heating of individual psoriatic lesions. This approach therefore constitutes a useful tool to provide realistic and individualized estimates of the physical effects of PDL (or other SPL-based) treatments of psoriatic plaques, which yields information that is essential in guiding experimental studies toward unraveling the remedial mechanisms of these treatments. This knowledge, in turn, is critical for the creation of patient-tailored treatment protocols capable of maximizing remission periods. Furthermore, we identified several suspected pathogenic processes which are likely stalled or arrested by the PDL-induced photothermal effects and, therefore, should be the subject of future experimental studies to determine their role in extending psoriasis remission periods.

AUTHOR CONTRIBUTIONS

Leah S. Wilk carried out calculations and analyzed the data. Meagan Doppegieter sectioned, labeled, and imaged the biopsies. Nick van der Beek was responsible for tissue acquisition and logistics. Ton G. van Leeuwen and Maurice C. G. Aalders supervised the project. All authors contributed to planning, design of experiments, discussion of results, and writing of the manuscript.

ACKNOWLEDGMENTS

The authors would like to thank E.N.T.P. Bakker and E. van Bavel for fruitful discussions.

CONFLICT OF INTEREST STATEMENT

The authors declare no conflict of interest.

DATA AVAILABILITY STATEMENT

All data needed to evaluate the conclusions in the paper are present in the paper and/or the Supplementary Materials.

ORCID

Leah S. Wilk  <http://orcid.org/0000-0002-4881-8552>

Meagan Doppegieter  <https://orcid.org/0000-0002-2217-7742>

REFERENCES

1. Parisi R, Iskandar IYK, Kontopantelis E, Augustin M, Griffiths CEM, Ashcroft DM. National, regional, and worldwide epidemiology of psoriasis: systematic analysis and modelling study. *BMJ*. 2020;369:m1590. <https://doi.org/10.1136/bmj.m1590>
2. Szepietowski JC, Reich A. Pruritus in psoriasis: an update. *Eur J Pain*. 2016;20(1):41–6. <https://doi.org/10.1002/ejp.768>
3. Sumpton D, Kelly A, Tunnicliffe DJ, Craig JC, Hassett G, Chessman D, et al. Patients' perspectives and experience of psoriasis and psoriatic arthritis: a systematic review and thematic synthesis of qualitative studies. *Arthritis Care Res*. 2020;72(5):711–22. <https://doi.org/10.1002/acr.23896>
4. Reich K, Mrowietz U, Radtke MA, Thaci D, Rustenbach SJ, Spehr C, et al. Drug safety of systemic treatments for psoriasis: results from The German Psoriasis Registry PsoBest. *Arch Dermatol Res*. 2015;307(10):875–83. <https://doi.org/10.1007/s00403-015-1593-8>
5. Bos JD, Spuls PI. Topical treatments in psoriasis: today and tomorrow. *Clin Dermatol*. 2008;26(5):432–7. <https://doi.org/10.1016/j.clindermatol.2007.10.025>
6. No DJ, Inkeles MS, Amin M, Wu JJ. Drug survival of biologic treatments in psoriasis: a systematic review. *J Dermatol Treat*. 2018;29(5):460–6. <https://doi.org/10.1080/09546634.2017.1398393>
7. Mason KJ, Williams S, Yiu ZZN, McElhone K, Ashcroft DM, Kleyen CE, et al. Persistence and effectiveness of nonbiologic systemic therapies for moderate-to-severe psoriasis in adults: a systematic review. *Br J Dermatol*. 2019;181(2):256–64. <https://doi.org/10.1111/bjd.17625>
8. Mehta D, Lim HW. Ultraviolet B phototherapy for psoriasis: review of practical guidelines. *Am J Clin Dermatol*. 2016;17(2):125–33. <https://doi.org/10.1007/s40257-016-0176-6>
9. Koo J, Lebwohl M. Duration of remission of psoriasis therapies. *J Am Acad Dermatol*. 1999;41:51–9. [https://doi.org/10.1016/S0190-9622\(99\)70406-8](https://doi.org/10.1016/S0190-9622(99)70406-8)
10. Collins L, Quinn A, Stasko T. Skin cancer and immunosuppression. *Dermatol Clin*. 2019;37(1):83–94. <https://doi.org/10.1016/j.det.2018.07.009>
11. Narayanan DL, Saladi RN, Fox JL. Review: Ultraviolet radiation and skin cancer. *Int J Dermatol*. 2010;49(9):978–86. <https://doi.org/10.1111/j.1365-4632.2010.04474.x>
12. Schwarz T. Mechanisms of UV-induced immunosuppression. *Keio J Med*. 2005;54(4):165–71. <https://doi.org/10.2302/kjm.54.165>
13. Zelickson BD, Mehregan DA, Wendelscher-Crabb G, Ruppman D, Cook A, O'Connell P, et al. Clinical and histologic evaluation of psoriatic plaques treated with a flashlamp pulsed dye laser. *J Am Acad Dermatol*. 1996;35:64–8. [https://doi.org/10.1016/S0190-9622\(96\)90498-3](https://doi.org/10.1016/S0190-9622(96)90498-3)
14. Momsen OH, Kiil J. Dermatome shaving of psoriasis seven years experience in 112 patients. *Scand J Plast Reconstr Surg Hand Surg*. 1993;27(2):143–7. <https://doi.org/10.3109/02844319309079798>

15. Taibjee SM, Cheung ST, Laube S, Lanigan SW. Controlled study of excimer and pulsed dye lasers in the treatment of psoriasis. *Br J Dermatol.* 2005;153(5):960–6. <https://doi.org/10.1111/j.1365-2133.2005.06827.x>
16. de Leeuw J, Tank B, Bjerring PJ, Koetsveld S, Neumann M. Concomitant treatment of psoriasis of the hands and feet with pulsed dye laser and topical calcipotriol, salicylic acid, or both: a prospective open study in 41 patients. *J Am Acad Dermatol.* 2006;54(2):266–71. <https://doi.org/10.1016/j.jaad.2005.07.072>
17. Ros A-M, Garden JM, Bakus AD, Hedblad M-A. Psoriasis response to the pulsed dye laser. *Lasers Surg Med.* 1996;19(3):331–5. [https://doi.org/10.1002/\(SICI\)1096-9101\(1996\)19:3%3C331::AID-LSM8%3E3.0.CO;2-T](https://doi.org/10.1002/(SICI)1096-9101(1996)19:3%3C331::AID-LSM8%3E3.0.CO;2-T)
18. Rox Anderson R, Parrish JA. Microvasculature can be selectively damaged using dye lasers: a basic theory and experimental evidence in human skin. *Lasers Surg Med.* 1981;1(3):263–76. <https://doi.org/10.1002/lsm.1900010310>
19. Svaasand LO, Fiskerstrand EJ, Kopstad G, Norvang LT, Svaasand EK, Nelson JS, et al. Therapeutic response during pulsed laser treatment of port-wine stains: dependence on vessel diameter and depth in dermis. *Lasers Med Sci.* 1995;10(4):235–43. <https://doi.org/10.1007/BF02133615>
20. Heidenreich R, Röcken M, Ghoreschi K. Angiogenesis drives psoriasis pathogenesis. *Int J Exp Pathol.* 2009;90(3):232–48. <https://doi.org/10.1111/j.1365-2613.2009.00669.x>
21. Lowes MA, Suárez-Fariñas M, Krueger JG. Immunology of psoriasis. *Annu Rev Immunol.* 2014;32:227–55. <https://doi.org/10.1146/annurev-immunol-032713-120225>
22. Soliman M, Zaher H, Danasouri NE, Attia A, Tawfik W. Effect of pulsed dye laser on intercellular adhesion molecule-1 (ICAM-1) expression after treatment of psoriasis. *Med Laser Appl.* 2011;26(1):20–6. <https://doi.org/10.1016/j.mla.2010.03.002>
23. Raychaudhuri SP, Jiang WY, Farber EM. Psoriatic keratinocytes express high levels of nerve growth factor. *Acta Derm Venereol.* 1998;78(2):84–6. <https://doi.org/10.1080/000155598433368>
24. Ostrowski SM, Belkadi A, Loyd CM, Diaconu D, Ward NL. Cutaneous denervation of psoriasisform mouse skin improves acanthosis and inflammation in a sensory neuropeptide-dependent manner. *J Invest Dermatol.* 2011;131(7):1530–8. <https://doi.org/10.1038/jid.2011.60>
25. Misery L. Skin, immunity and the nervous system. *Br J Dermatol.* 1997;137(6):843–50. <https://doi.org/10.1111/j.1365-2133.1997.tb01542.x>
26. Sweeney CM, Tobin AM, Kirby B. Innate immunity in the pathogenesis of psoriasis. *Arch Dermatol Res.* 2011;303(10):691–705. <https://doi.org/10.1007/s00403-011-1169-1>
27. Sabat R, Philipp S, Höflich C, Kreutzer S, Wallace E, Asadullah K, et al. Immunopathogenesis of psoriasis. *Exp Dermatol.* 2007;16(10):779–98. <https://doi.org/10.1111/j.1600-0625.2007.00629.x>
28. Lepock JR. Cellular effects of hyperthermia: relevance to the minimum dose for thermal damage. *Int J Hyperthermia.* 2003;19(3):252–66. <https://doi.org/10.1080/0265673031000065042>
29. He X, Wolkers WF, Crowe JH, Swanlund DJ, Bischof JC. In situ thermal denaturation of proteins in dunning AT-1 prostate cancer cells: implication for hyperthermic cell injury. *Ann Biomed Eng.* 2004;32(10):1384–98. <https://doi.org/10.1114/B:ABME.000042226.97347.de>
30. Grüter T, Blusch A, Motte J, Sgodzai M, Bachir H, Klimas R, et al. Immunomodulatory and anti-oxidative effect of the direct TRPV1 receptor agonist capsaicin on Schwann cells. *J Neuroinflammation.* 2020;17(1):145. <https://doi.org/10.1186/s12974-020-01821-5>
31. Yuan Y, Yan S, Fang Q. Light transport modeling in highly complex tissues using the implicit mesh-based Monte Carlo algorithm. *Biomed Opt Express.* 2021;12(1):147–61. <https://doi.org/10.1364/BOE.411898>
32. Bradley D, Roth G. Adaptive thresholding using the integral image. *J Graph Tools.* 2007;12(2):13–21. <https://doi.org/10.1080/2151237X.2007.10129236>
33. Gonzalez RC, Woods RE, Eddins SL. Digital image processing using MATLAB. New Jersey: Pearson Prentice Hall; 2004.
34. M Moerman K. GIBBON: the geometry and image-based bioengineering add-on. *J Open Source Softw.* 2018;3(22):506.
35. Patterson MS, Chance B, Wilson BC. Time resolved reflectance and transmittance for the non-invasive measurement of tissue optical properties. *Appl Opt.* 1989;28(12):2331–6. <https://doi.org/10.1364/AO.28.002331>
36. van Gemert MJC, Welch AJ, Pickering JW, Tan OT, Gijssbers GHM. Wavelengths for laser treatment of port wine stains and telangiectasia. *Lasers Surg Med.* 1995;16(2):147–55.
37. Welch AJ, van Gemert MJC. Optical-thermal response of laser-irradiated tissue. Berlin: Springer; 2011.
38. Orgill DP, Solari MG, Barlow MS, O'Connor NE. A finite-element model predicts thermal damage in cutaneous contact burns. *J Burn Care Rehabil.* 1998;19(3):203–9. <https://doi.org/10.1097/00004630-199805000-00003>
39. Nellis G, Klein SA. Heat transfer. Cambridge: Cambridge University Press; 2008.
40. Marieb EN, Hoehn K. Human anatomy & physiology. San Francisco: Benjamin Cummings; 2008.
41. Holzer P. The pharmacological challenge to tame the transient receptor potential vanilloid-1 (TRPV1) nociceptor. *Br J Pharmacol.* 2008;155(8):1145–62. <https://doi.org/10.1038/bjp.2008.351>
42. Caterina MJ, Rosen TA, Tominaga M, Brake AJ, Julius D. A capsaicin-receptor homologue with a high threshold for noxious heat. *Nature.* 1999;398(6726):436–41. <https://doi.org/10.1038/18906>
43. Pickering JW, Butler PH, Ring BJ, Walker EP. Thermal profiles of blood vessels heated by a laser. *Australas Phys Eng Sci Med.* 1989;12(1):11–5.
44. Doppegieter M, van der Beek N, Bakker ENTP, Neumann MHA, van Bavel E. Effects of pulsed dye laser treatment in psoriasis: a nerve-wrecking process? *Exp Dermatol.* 2023;32(7):1165–73. <https://doi.org/10.1111/exd.14816>
45. Zhu TH, Nakamura M, Farahnik B, Abrouk M, Lee K, Singh R, et al. The role of the nervous system in the pathophysiology of psoriasis: a review of cases of psoriasis remission or improvement following denervation injury. *Am J Clin Dermatol.* 2016;17(3):257–63. <https://doi.org/10.1007/s40257-016-0183-7>
46. Westcott EB, Segal SS. Perivascular innervation: a multiplicity of roles in vasomotor control and myoendothelial signaling. *Microcirculation.* 2013;20(3):217–38. <https://doi.org/10.1111/micc.12035>
47. Henning JPH, van Gemert MJC, Lahaye CTW. Clinical and histological evaluation of portwine stain treatment with a microsecond-pulsed dye-laser at 577 NM. *Lasers Surg Med.* 1984;4(4):375–80. <https://doi.org/10.1002/lsm.1900040410>
48. Szydłowska K, Tymianski M. Calcium, ischemia and excitotoxicity. *Cell Calcium.* 2010;47(2):122–9. <https://doi.org/10.1016/j.ceca.2010.01.003>
49. Nattkemper LA, Tey HL, Valdes-Rodriguez R, Lee H, Mollanazar NK, Albornoz C, et al. The genetics of chronic itch: gene expression in the skin of patients with atopic dermatitis and psoriasis with severe itch. *J Invest Dermatol.* 2018;138(6):1311–7. <https://doi.org/10.1016/j.jid.2017.12.029>
50. Bernstein JE, Parish LC, Rapaport M, Rosenbaum MM, Roenigk HH. Effects of topically applied capsaicin on moderate and severe psoriasis vulgaris. *J Am Acad Dermatol.* 1986;15(3):504–7. [https://doi.org/10.1016/S0190-9622\(86\)70201-6](https://doi.org/10.1016/S0190-9622(86)70201-6)
51. González-Ramírez R, Chen Y, Liedtke WB, Morales-Lázaro SL. TRP channels and pain. In: Emir T, editor. *Neurobiology of TRP channels*. Boca Raton, FL: CRC Press/Taylor & Francis; 2017.

52. Yin N, Choudhary S, Nouri K. Pulsed dye laser for the treatment of nail psoriasis. *Cutis*. 2013;92(3):129–35.
53. Sánchez-Moreno A, Guevara-Hernández E, Contreras-Cervera R, Rangel-Yescas G, Ladrón-de-Guevara E, Rosenbaum T, et al. Irreversible temperature gating in trpv1 sheds light on channel activation. *Elife*. 2018;7:e36372. <https://doi.org/10.7554/eLife.36372>
54. Pushkareva AE, Ponomarev IV, Isaev AA, Klyuchareva SV. Numerical investigation of vessel heating using a copper vapor laser and a pulsed dye laser in treating vascular skin lesions. *Laser Phys*. 2018;28(2):025604. <https://doi.org/10.1088/1555-6611/aa8cdb>
55. Paul BS, Anderson RR, Jarve J, Parrish JA. The effect of temperature and other factors on selective microvascular damage caused by pulsed dye laser. *J Invest Dermatol*. 1983;81(4):333–6. <https://doi.org/10.1111/1523-1747.ep12519832>
56. Kuo YR, Wu WS, Jeng SF, Wang FS, Huang HC, Lin CZ, et al. Suppressed TGF- β 1 expression is correlated with up-regulation of matrix metalloproteinase-13 in keloid regression after flashlamp pulsed-dye laser treatment. *Lasers Surg Med*. 2005;36(1):38–42. <https://doi.org/10.1002/lsm.20104>
57. Cattin A-L, Burden JJ, Van Emmenis L, Mackenzie FE, Hoving JJA, Garcia Calavia N, et al. Macrophage-induced blood vessels guide Schwann cell-mediated regeneration of peripheral nerves. *Cell*. 2015;162(5):1127–39. <https://doi.org/10.1016/j.cell.2015.07.021>
58. Hern S, Allen MH, Sousa AR, Harland CC, Barker JNWN, Levick JR, et al. Immunohistochemical evaluation of psoriatic plaques following selective photothermolysis of the superficial capillaries. *Br J Dermatol*. 2001;145(1):45–53. <https://doi.org/10.1046/j.1365-2133.2001.04280.x>
59. Hohenleutner U, Hilbert M, Wlotzke U, Landthaler M. Epidermal damage and limited coagulation depth with the flashlamp-pumped pulsed dye laser: a histochemical study. *J Invest Dermatol*. 1995;104(5):798–802. <https://doi.org/10.1111/1523-1747.ep12606996>
60. Morsy H, Kamp S, Thrane L, Behrendt N, Saunderson B, Zayan H, et al. Optical coherence tomography imaging of psoriasis vulgaris: correlation with histology and disease severity. *Arch Dermatol Res*. 2010;302(2):105–11. <https://doi.org/10.1007/s00403-009-1000-4>
61. Aguirre J, Schwarz M, Garzorz N, Omar M, Buehler A, Eyerich K, et al. Precision assessment of label-free psoriasis biomarkers with ultra-broadband optoacoustic mesoscopy. *Nat Biomed Eng*. 2017;1(5):0068. <https://doi.org/10.1038/s41551-017-0068>
62. Rossmanna C, Haemmerich D. Review of temperature dependence of thermal properties, dielectric properties, and perfusion of biological tissues at hyperthermic and ablation temperatures. *Crit Rev Biomed Eng*. 2014;42(6):467–92. <https://doi.org/10.1615/critrevbiomedeng.2015012486>
63. Iorizzo TW, Jermain PR, Salomatina E, Muzikansky A, Yaroslavsky AN. Temperature induced changes in the optical properties of skin in vivo. *Sci Rep*. 2021;11(1):754. <https://doi.org/10.1038/s41598-020-80254-9>
64. Barton JK. Dynamic changes in optical properties. In: Welch AJ, van Gemert MJC, editors. *Optical-thermal response of laser-irradiated tissue*. Dordrecht: Springer Netherlands; 2011. p. 321–49. https://doi.org/10.1007/978-90-481-8831-4_9
65. Majaron B, Nelson JS. Laser treatment of port wine stains. In: Welch AJ, van Gemert MJC eds. *Optical-thermal response of laser-irradiated tissue*. Dordrecht: Springer Netherlands; 2011. p. 859–913. https://doi.org/10.1007/978-90-481-8831-4_23
66. Hielscher AH, Alcouffe RE, Barbour RL. Comparison of finite-difference transport and diffusion calculations for photon migration in homogeneous and heterogeneous tissues. *Phys Med Biol*. 1998;43(5):1285–302. <https://doi.org/10.1088/0031-9155/43/5/017>
67. Singh S, Melnik R. Thermal ablation of biological tissues in disease treatment: a++6+ review of computational models and future directions. *Electromagn Biol Med*. 2020;39(2):49–88. <https://doi.org/10.1080/15368378.2020.1741383>
68. Kumar S, Srivastava A. Thermal analysis of laser-irradiated tissue phantoms using dual phase lag model coupled with transient radiative transfer equation. *Int J Heat Mass Transfer*. 2015;90:466–79. <https://doi.org/10.1016/j.ijheatmasstransfer.2015.06.077>
69. Bhowmik A, Repaka R, Mishra SC, Mitra K. Analysis of radiative signals from normal and malignant human skins subjected to a short-pulse laser. *Int J Heat Mass Transfer*. 2014;68:278–94. <https://doi.org/10.1016/j.ijheatmasstransfer.2013.09.032>
70. Liao G, Xue J. Moving meshes by the deformation method. *J Comput Appl Math*. 2006;195(1):83–92. <https://doi.org/10.1016/j.cam.2005.07.022>
71. Tyfa Z, Obidowski D, Reorowicz P, Stefańczyk L, Fortuniak J, Józwick K. Numerical simulations of the pulsatile blood flow in the different types of arterial fenestrations: comparable analysis of multiple vascular geometries. *Biocybernet Biomed Eng*. 2018;38(2):228–42. <https://doi.org/10.1016/j.bbe.2018.01.004>
72. Lintzeri DA, Karimian N, Blume-Peytavi U, Kottner J. Epidermal thickness in healthy humans: a systematic review and meta-analysis. *J Eur Acad Dermatol Venereol*. 2022;36(8):1191–200. <https://doi.org/10.1111/jdv.18123>
73. Pasyk KA, Thomas SV, Hassett CA, Cherry GW, Faller R. Regional differences in capillary density of the normal human dermis. *Plast Reconstr Surg*. 1989;83(6):939–45.
74. Petrofsky JS, III EL, Suh HJ, et al. The effect of aging on conductive heat exchange in the skin at two environmental temperatures. *Med Sci Monit*. 2006;12(10):400–8.
75. Evans LC. *Partial differential equations*. Providence, RI: American Mathematical Society; 2010.
76. Cattaneo C. A form of heat-conduction equations which eliminates the paradox of instantaneous propagation. *Comptes Rendus*. 1958;247:431.
77. Vernotte P. Les paradoxes de la theorie continue de l'equation de la chaleur. *Comptes Rendus*. 1958;246:3154–5.
78. Xu F, Lu TJ, Seffen KA, Ng EYK. Mathematical modeling of skin bioheat transfer. *Appl Mech Rev*. 2009;62(5):050801. <https://doi.org/10.1115/1.3124646>
79. Moritz AR, Henriques FC. Studies of thermal injury: II. the relative importance of time and surface temperature in the causation of cutaneous burns. *Am J Pathol*. 1947;23(5):695–720.
80. Pearce JA. Comparative analysis of mathematical models of cell death and thermal damage processes. *Int J Hyperthermia*. 2013;29(4):262–80. <https://doi.org/10.3109/02656736.2013.786140>
81. Lukač M, Lozar A, Perhavec T, Bajd F. Variable heat shock response model for medical laser procedures. *Lasers Med Sci*. 2019;34(6):1147–58. <https://doi.org/10.1007/s10103-018-02704-1>
82. Lepock JR. How do cells respond to their thermal environment? *Int J Hyperthermia*. 2005;21(8):681–7. <https://doi.org/10.1080/02656730500307298>
83. Thomsen S, Pearce JA. Thermal damage and rate processes in biologic tissues. In: Welch AJ, van Gemert MJC, editors. *Optical-thermal response of laser-irradiated tissue*. Dordrecht: Springer Netherlands; 2011. p. 487–549.
84. Elmets CA, Lim HW, Stoff B, Connor C, Cordoro KM, Lebwohl M, et al. Joint American Academy of Dermatology—National Psoriasis Foundation guidelines of care for the management and treatment of psoriasis with phototherapy. *J Am Acad Dermatol*. 2019;81(3):775–804. <https://doi.org/10.1016/j.jaad.2019.04.042>
85. Grazielle Quadros B, Marques Glen C, Neres D, Stachelski RA, Buzanello MR, Bertolini GRF. Therapeutic effects of laser on psoriasis plaques: a systematic review. *J Cosmet Laser Ther*. 2023;25(5–8):65–73. <https://doi.org/10.1080/14764172.2023.2241691>

86. Mattei PL, Corey KC, Kimball AB. Psoriasis Area Severity Index (PASI) and the Dermatology Life Quality Index (DLQI): the correlation between disease severity and psychological burden in patients treated with biological therapies. *J Eur Acad Dermatol Venereol*. 2014;28(3):333–7. <https://doi.org/10.1111/jdv.12106>
87. Perrott SB, Murray AH, Lowe J, Mathieson CM. The psychosocial impact of psoriasis: physical severity, quality of life, and stigmatization. *Physiol Behav*. 2000;70(5):567–71. [https://doi.org/10.1016/S0031-9384\(00\)00290-0](https://doi.org/10.1016/S0031-9384(00)00290-0)

How to cite this article: Wilk LS, Doppegieter M, Beek N, Leeuwen TG, Aalders MCG. Modeling pulsed dye laser treatment of psoriatic plaques by combining numerical methods and image-derived lesion morphologies. *Lasers Surg Med*. 2024;56:508–22. <https://doi.org/10.1002/lsm.23781>